Journal of Statistical Mechanics: Theory and Experiment
An IOP and SISSA journal

PAPER: Classical statistical mechanics, equilibrium and non-equilibrium

Exploring transitions in finite-size Potts model: comparative analysis using Wang–Landau sampling and parallel tempering

Fangfang Wang[1,5,6], **Wei Liu**[2,*], **Jun Ma**[1,5,6], **Kai Qi**[3,*], **Ying Tang**[4,1] **and Zengru Di**[1,5,6]

[1] Department of Systems Science, Faculty of Arts and Sciences, Beijing Normal University, Zhuhai 519087, People's Republic of China
[2] College of Science, Xi'an University of Science and Technology, Xi'an, People's Republic of China
[3] 2020 X-Lab, Shanghai Institute of Microsystem and information Technology, Chinese Academy of Sciences, Shang Hai, People's Republic of China
[4] Institute of Fundamental and Frontier Sciences, University of Electronic Sciences and Technology of China, Chengdu 611731, People's Republic of China
[5] International Academic Center of Complex Systems, Beijing Normal University, Zhu Hai 519087, People's Republic of China
[6] School of Systems Science, Beijing Normal University, Beijing 100875, People's Republic of China
E-mail: weiliu@xust.edu.cn and kqi@mail.sim.ac.cn

Received 18 June 2024
Accepted for publication 23 August 2024
Published 9 September 2024

Online at stacks.iop.org/JSTAT/2024/093201
https://doi.org/10.1088/1742-5468/ad72da

Abstract. This research provides a examination of transitions within the various-state Potts model in two-dimensional finite-size lattices. Leveraging the Wang–Landau sampling and parallel tempering, we systematically obtain the density of states, facilitating a comprehensive comparative analysis of the results. The determination of the third-order transitions location are achieved through a meticulous examination of the density of states using microcanonical inflection-point analysis. The remarkable alignment between canonical and microcanonical

*Authors to whom any correspondence should be addressed.

results for higher-order transition locations affirms the universality of these transitions. Our results further illustrate the universality of the robust and microcanonical inflection-point analysis of Wang–Landau sampling.

Keywords: Potts model, third-order transitions, Wang–Landau sampling, parallel tempering, microcanonical inflection-point analysis

Contents

1. Introduction

Traditional statistical physics and thermodynamics has achieved great success in explaining the thermodynamic behavior of macroscopic systems. Phase transitions are cooperative phenomena associated with many factors such as temperature and pressure. The structure and physical properties of the system will change as certain parameters (primarily temperature) change continuously [1]. The study of phase transitions have a long history. Most prior research had focused on phase transitions in macroscopic systems, meaning that the size of systems was infinitely large, for example, the exact solution of the two-dimensional Ising model [2], Landau's theory of phase transitions [3], and Wilson's Renormalization group theory [4]. However, in reality, systems are not always infinitely large [5]. Many systems in nature and synthetic materials are of finite scale, such as nanomaterials [6], living systems, social systems, and complex systems [7], among others. The scale and microstructure of these small systems have significant impacts on the thermodynamic and dynamic behaviors, so that the phase transitions of the small systems exhibit different behaviors from those of the infinite systems [8]. Traditional phase transitions discuss the singularity of thermodynamic quantities, which

J. Stat. Mech. (2024) 093201

are absent in finite systems [9]. As a consequence, a different definition for phase transitions in finite systems is demanded.

The microcanonical analysis has been employed for the identification of phase transitions in the past few decades [10, 11]. Recently the microcanonical inflection-point analysis (MIPA) has emerged as a powerful tool for studying phase transitions in finite-size systems. It has been further generalized by Qi and Bachmann [12] to identify higher-order transitions, among which independent and dependent transitions can be distinguished. The inflection point of the higher-order derivative of microcanonical entropy, being the least sensitive, accurately marks the precise location where the monotonicity of the corresponding function changes. Independent transition resemble traditional phase transitions and occur independently of other collaborative activities within the system. In contrast, dependent transition rely on the occurrence of lower-order phase transitions. These transitions manifest at higher energy levels and are of a higher-order than the independent transitions they accompany. Using the exact density of states (DOS) of the Ising model [13], Sitarachu studied the 1D and 2D finite-size Ising model in detail [14], where higher-order transitions were identified in the 2D system. They also found that the physical significance of the third-order dependent transition is the location where the size of the group condenses the fastest, and is a precursor to the critical phase transition. Additionally, MIPA has been successfully applied to studies of nanomaterials, flexible polymers, and the Baxter–Wu model [14–18]. The outcomes of these studies elucidate major transitions and further detail the transformation process by indicating higher-order transitions. Moreover, it has proven effective in accurately identifying phase transition energies, characterizing phase transitions of various orders [19], and is also applicable in discerning different structural phases and constructing suitable parametric hyperphase diagrams [20].

The Potts model, originally proposed by Potts in 1952 [21], is an extension of the Ising model [22] and incorporates more than two states. Historically overlooked, this model has gained increasing attention over the last decade due to its rich structure and relevance to numerous fundamental issues in statistical physics. The Potts model is notably linked with significant challenges in lattice statistics, and its critical behavior has proven to be richer and more encompassing than that of the Ising model. As a vital platform for testing various methods and approaches, the Potts model has significantly contributed to theoretical research [23, 24], and has many applications in complex networks, such as community structure [25], protein folding networks [26], and networks connecting music groups and audiences [27]. It is also widely used in the social sciences [28], cellular biology [29], computational biology [30], and image processing [31].

Given that the Potts model lacks a precisely defined the DOS, it is necessary to obtain the DOS through simulation. Wang–Landau sampling (WL) [32] and parallel tempering (PT) [33] are two Monte Carlo methods widely utilized in statistical physics, each offering unique advantages and limitations. WL efficiently generates the DOS map by dynamically adjusting the sampling probability, facilitating the rapid calculation of thermodynamic properties across various temperatures. This method is particularly effective for sampling complex energy landscapes but can suffer from difficult-to-control convergence, sensitivity to parameter selection, and complexity in implementation. In contrast, PT addresses the challenge of local minima by exchanging configurations

J. Stat. Mech. (2024) 093201

between multiple temperature layers, making it well-suited for systems characterized by multiple energy minima, such as Spin Glass Simulations [34] and protein folding [33]. While inherently suited for parallel computing, this method demands significant computational resources, and the selection of parameters, such as appropriate temperature intervals, is crucial for its efficiency. Consequently, we employed both WL and PT methods to determine the DOS of the systems.

In this paper, the DOS of the Potts model is obtained with the WL and PT, and the position of the higher-order transitions are determined, demonstrating the universal existence of higher-order transitions. In section 2, we briefly describe the model and methodology. Section 3 presents and discusses the results, while the final section summarizes our work.

2. The model and the method

2.1. Potts model

The Hamiltonian built on the $N \times N$ square lattices is as follows,

$$E = -J \sum_{<ij>} \delta(\sigma_i, \sigma_j), \tag{1}$$

where σ_i stands for the spin located in the square lattices, and $< i, j >$ denotes the summations over the nearest neighbor sites. σ_i can take q discrete values: $0, 1, \ldots, q-1$. If the spins of two neighbors are the same, an interacting potential energy $-J$ is added to the total potential energy for two identical neighboring spins. Otherwise, no net contribution occurs. A single spin flip typically leads to a $4J$ energy difference. There are two exceptions: the differences between the ground state and the first excited state, and between the highest energy level and the second-to-last energy level are $8J$. As a result, there are $4N^2 + 1$ energy levels in this model.

2.2. Wang–Landau sampling

We can obtain $g(E)$ using WL, a sophisticated Monte Carlo method [32]. $g(E)$ is estimated through a random walk in energy space once the histogram becomes flat. We start with $g(E) = 1$ and improve it as follows: the random walk proceeds according to a specified probability distribution.

$$p(E_1 \to E_2) = \min\left(\frac{g(E_1)}{g(E_2)}, 1\right), \tag{2}$$

where E_1 and E_2 is the energy level before and after spin flipping, the density of states is updated by

$$g(E) \to g(E) f, \tag{3}$$

Where E is the energy level of the accepted state, and f is a modification factor, with an initial value set to $f = f_0 = e = 2.718\,28$. Simultaneously, the energy histogram

J. Stat. Mech. (2024) 093201

$H(E)$ is incremented by 1. We proceed with the random walks until the histogram of energies becomes 'flat,' defined as each energy level's histogram being at least 80% of the average histogram value. Then, the modification factor is reduced to $f_{i+1} = f_i^{1/2}$, the histogram is reset to $H(E) = 0$ for all values of E, and the random walks are restarted. The simulation terminates when the modification factor falls below $f_{\text{final}} = 1 + 10^{-8}$.

The primary advantage of this method is that it avoids critical slowing down. However, as the system size and the complexity of the model increase, sampling the full energy range becomes challenging, resulting in prolonged periods required to achieve a flat energy histogram [35]. Therefore, Vogel *et al* proposed replica-exchange Wang Landau sampling [36, 37], which is ideally suited for studying complex, large systems. In this method, energy levels are partitioned into overlapping sub-windows across multiple adjacent windows. In this study, samples are collected from multiple independent walking sub-windows, with 75% of the overlapping sections being selected. Given the specified number of Monte Carlo steps, two random walks are chosen for exchange

$$P_{\text{acc}} = \min\left[1, \frac{g_i(E(\{s_i\})g_j(E(\{s_j\})}{g_i(E(\{s_j\})g_j(E(\{s_i\})}\right]. \tag{4}$$

To calculate a single $g(E)$ across the entire energy range, we chose the joining point for any two overlapping densities of states where the microcanonical inverse temperature $\beta = \mathrm{d}\log[g(E)]/\mathrm{d}E$ best coincide. Convergence of $g(E)$ is accelerated within the smaller energy range of the sub-window.

2.3. Parallel tempering

To cross-verify the DOS obtained by WL, we calculate the DOS using PT to ensure accuracy and consistency between different computational methods. The low-temperature phases of finite-sized lattices and other complex systems typically feature numerous local minima, each separated by energy barriers. To comprehensively study these systems, it is essential to analyze each configuration of these local minima and the associated fluctuations. The PT method is a technique for optimizing complex systems and sampling intricate probability distributions, particularly for energy functions with multiple local minima [33, 38]. The PT algorithm operates as follows: (1). Initialization: create multiple replicas at different temperatures, each representing the system's state at a specific temperature. Typically, the temperature sequence ranges from the lowest temperature (near 0) to the highest temperature (usually near or above the phase transition point) in a geometric progression. (2). Independent sampling: each chain is sampled independently according to its temperature using the Metropolis algorithm.(3). Exchange steps: periodically attempt to exchange states between adjacent temperature chains. The exchange probability is determined by the Metropolis criterion to ensure the system's detailed balance. For two adjacent chains i and j (with i having a lower temperature), the exchange probability P is given by $P = \min(1, \mathrm{e}^{(\beta_i - \beta_j)(E_j - E_i)})$, where $\beta_i = 1/k_{\text{B}}T_i$ is the inverse temperature and E is the energy of chain i. (4). Iteration:

J. Stat. Mech. (2024) 093201

repeat steps (2) and (3) until a predetermined number of iterations or convergence criteria is reached. We use 30 temperature intervals for each size in each state for temperature exchange, ultimately obtaining the energy histogram corresponding to each temperature. The DOS of the system is then derived through the multi-histogram algorithm [38].

$$\hat{g}(E) = \frac{\sum_{i=1}^{I} h_i(E)}{\sum_{i=1}^{I} M_i Z_i^{-1} \mathrm{e}^{-\beta_i E}}, \tag{5}$$

where the partition function is,

$$Z_i = \sum_{E} \hat{g}(E) \mathrm{e}^{-\beta_i E}, \tag{6}$$

where $g(E)$ is DOS, $h_i(E)$ is the number of energy histograms at the ith temperature. By iteratively applying equations (5) and (6), the DOS of the system can be obtained.

2.4. Microcanonical infection-point analysis method

Qi and Bachmann combined microcanonical analysis with the principle of minimum sensitivity to identify and classify first- and higher-order transitions in complex systems [12]. Through this analysis, they discovered that the phase transition signals exhibited by the two-dimensional ferromagnetic Ising model represent not only simple second-order phase transitions but also more complex behaviors. Third-order independent and dependent transitions are also observed in the system. Additionally, they obtained a phase diagram that illustrates the interaction of the fibrous polymer with the adhesive surface.

The macroscopic behavior of a physical system is governed by entropy and energy, while microcanonical entropy, encompassing all information about the phase behavior of the system, can be defined as follows:

$$S(E) = k_{\mathrm{B}} \ln g(E), \tag{7}$$

where k_{B} is the Boltzmann constant, $S(E)$ represents entropy and its derivatives are monotone functions within the energy region associated with a single phase. However, phase transitions disrupt this monotonicity and introduces an inflection point.

According to the principle of least sensitivity, the least sensitive inflection point possesses physical significance. For example, if $S(E)$ has a least-sensitive inflection point, its first derivative is

$$\beta(E) = T^{-1}(E) = \frac{\mathrm{d}S(E)}{\mathrm{d}E}, \tag{8}$$

where $\beta(E)$, representing the microcanonical inverse temperature, should exhibit a positive minimum. This indicates a first-order phase transition. If $\beta(E)$ exhibits a least-sensitive inflection point, its first derivative can be obtained by

$$\gamma(E) = \frac{\mathrm{d}\beta(E)}{\mathrm{d}E} = \frac{\mathrm{d}^2 S(E)}{\mathrm{d}E^2}, \tag{9}$$

J. Stat. Mech. (2024) 093201

where $\gamma(E)$, describing the rate of change of the microcanonical inverse temperature, can reveal information about first and second order transitions. Furthermore,

$$\delta(E) = \frac{\mathrm{d}\gamma(E)}{\mathrm{d}E} = \frac{\mathrm{d}^3 S(E)}{\mathrm{d}E^3}, \tag{10}$$

where $\delta(E)$ represents the third derivative of $S(E)$ with respect to E, can reveal information about third-order transitions. In addition to the class of independent transition, another category of dependent transition can also be identified by this method.

Derivatives based directly on discrete microcanonical entropy are influenced by the noise associated with numerical errors in the data. To avoid the noise, we employ a two-step strategy. The first step is straightforward, we compute DOS 10 times and then average these calculations to obtain a smoother curve. Next, we utilize the Bézier algorithm to generate a smooth function [39]. The discrete data points f_q at energy E_q, obtained from WL, serve as control points in the derivatives of the microcanonical entropy.

$$f_{\mathrm{bez}} = \sum_{q=0}^{Q} C_Q^q \left(\frac{E_Q - E}{E_Q - E_0}\right)^{Q-q} \left(\frac{E - E_0}{E_Q - E_0}\right)^{q} f_q, \tag{11}$$

where q and Q represent the current energy level and the highest energy level, respectively, and E_0 is the energy of the ground state. f_q denotes variables such as S_q, β_q, γ_q, or δ_q. The derivatives required for the statistical analysis are calculated from these variables, as detailed in this study. We also perform ten independent computations to determine the error bars. If the error bars are not visible, they are smaller than the symbols used in the figures.

3. Results

3.1. Traditional transitions

The objective of this study is to determine the order of phase transitions in the finite-size Potts model for various values of q. We conducted simulations for $q = 3, 4, 6$ and 8 across system sizes ranging from $N = 16$ to 56. DOS data were obtained using replica exchange WL and PT, and the phase transition points were identified through canonical analysis and MIPA. First, the results comparing WL and PT for the DOS of the Potts model with $N = 32$ for $q = 3$ are shown in figure 1. The inset in the figure provides an analysis of the relative errors between WL and PT.

We observe that the results obtained from these two methods are in close agreement, which provides validation for the accuracy of the data obtained via WL. Next, we used the DOS obtained by WL for MIPA, and identified the positions of phase transition points in Potts model of various states. We calculate the specific heat values in the system using the formula

$$c_V = \frac{< E^2 > - < E >^2}{N^2 k_{\mathrm{B}} T^2}, \tag{12}$$

J. Stat. Mech. (2024) 093201

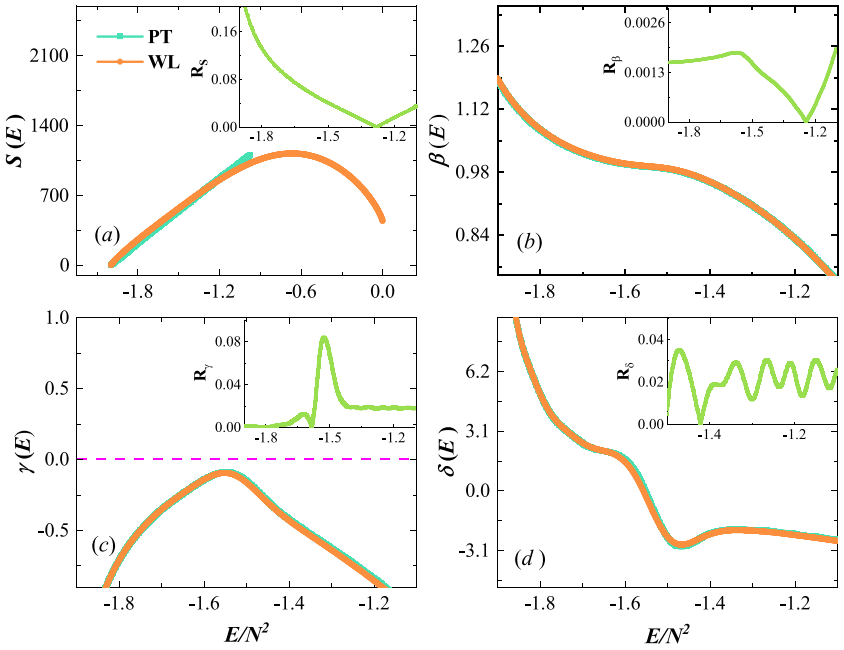

Figure 1. Microcanonical entropy per spin $S(E)$ ($S(E) = k_{\mathrm{B}} \ln g(E)$) and its derivatives $(b)\beta(E)$, $(c)\gamma(E)$ and $(d)\delta(E)$ for $N = 32$, $q = 3$ plotted as functions of the energy per spin $e = E/N^2$ obtained by WL and PT. The small picture is the relative error of the logarithm of the $S(E)$, $\beta(E)$, $\gamma(E)$ and $\delta(E)$ are R_S, R_β, R_γ and R_δ by WL and PT.

where $< E^n >= \sum_E E^n g(E) \mathrm{e}^{-E/k_{\mathrm{B}}T}$. The locations of the transition points are determined by the peaks in the specific heat. To reaffirm the accuracy of the DOS, we conduct a finite size analysis of the specific heat to determine the critical exponents α/ν. Figure 2 presents the finite size analysis of the specific heat in the Potts model under different states. By determining the maximum specific heat, $\ln c_V = (\alpha/\nu) \times \ln N$ can be obtained according to $c_V = N^{\alpha/\nu}$, thus the slope of the curve represents the critical exponents α/ν that we need. Therefore, for $q = 3$, the value of the key index $\alpha/\nu = 0.396$, and for $q = 4$, $\alpha/\nu = 0.996$. In the Potts model reported by [23], the critical exponent $\alpha/\nu = 0.4$ when $q = 3$, and $\alpha/\nu = 1$ when $q = 4$. Our results closely match the exact solution, and the DOS derived by WL shows satisfactory agreement. Based on this, the MIPA method, based on DOS, identifies the position of the third order transitions.

The phase transition points of the Potts model were determined by Baxter using the transfer matrix method [24], the result is $T_c = 1/\ln(1+\sqrt{q})$. Consequently, the phase transition temperatures for $q = 3, 4, 6$ and 8 are $T_c(3) \approx 0.995$, $T_c(4) \approx 0.910$, $T_c(6) \approx 0.808$ and $T_c(8) \approx 0.745$ respectively. According to MIPA, the temperature corresponding to the energy level at the maximum value of the curve $\gamma(E)$ in $\beta(E)$ indicates the temperature at which a traditional phase transition occurs. The transition temperatures under canonical and microcanonical analysis conditions are obtained respectively, as shown in table 1. The obtained transition temperatures closely approximate the exact values, which corroborates the accuracy of the DOS and provides a solid foundation for precisely identifying the locations of third-order transitions. In the table, the first line

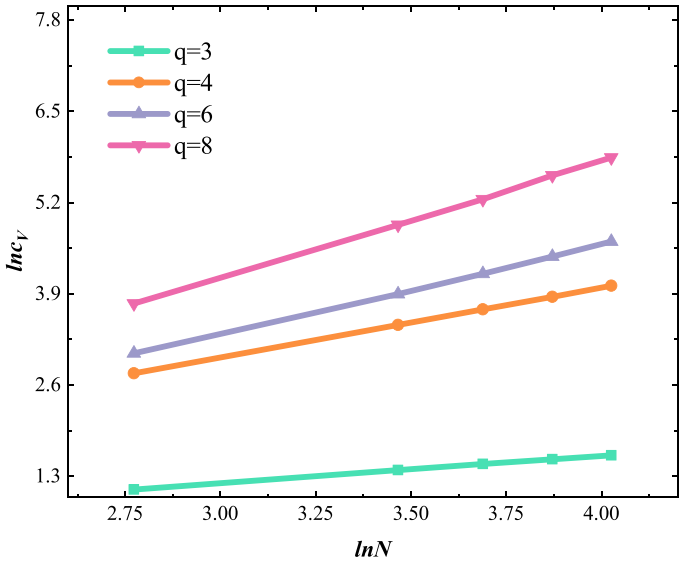

Figure 2. The specific heat in finite size analysis of Potts model under $q = 3, 4, 6$ and 8 states from $N = 16 - 56$. It shows the relationship between the logarithm of the maximum specific heat of different states and the logarithm of dimensions, and the slope is the critical exponent α/ν.

represents the phase transition temperatures obtained from specific heat, the second line represents the phase transition temperatures obtained by MIPA, and the energy level corresponding to the phase transition points are shown in parentheses. The temperature of the transitions gradually decrease with the increase of q.

Figures 3(a) and (d) give the microcanonical inverse temperature $\beta(E)$ (which is also the first derivative of the entropy $S(E)$ with respect to energy) with the energy level e. (b), (e) and (c), (f) are $\gamma(E)$ and $\delta(E)$ for the second and third derivative of the microcanonical entropy with respect to energy, respectively. In figure 3(b), a negative maximum value is observed on the curve $\gamma(E)$ for $q = 4$. Combined with the summary provided in table 2, this observation confirms that the 4-state Potts model undergoes a second-order transition at finite size. This finding aligns with the established understanding of second-order phase transitions in Potts model for $q < 5$. Similarly, the positive extreme value of $\gamma(E)$ observed in figure 3(e) indicates that the Potts model with $q = 6$ undergoes a first-order phase transition in finite-size systems. The non-monotone backbending trend of $\beta(E)$ observed in figure 3(d) is also a typical signal of a first-order phase transition.

3.2. Third order transitions

We locate the third-order transition points using the curve $\delta(E)$. Figure 3 illustrates the MIPA for the $q = 4$ and $q = 6$ states of the Potts model. Figures 3(a)–(c) presents the results of the MIPA for the Potts model with $q = 4$. According to the conclusions drawn from the MIPA, identifying the negative maximum and positive minimum values on the curve $\delta(E)$ allows for the determination of the energy levels associated with

Table 1. Microcanonical analysis and canonical analysis results of different q.

		$N=16$	$N=32$	$N=40$	$N=48$	$N=56$
$1/\ln(1+\sqrt{3})\approx 0.995$						
$q=3$	$1/\beta_c$	1.013	1.003	1.001	1.000	0.999
	$1/\beta_m$	1.024	1.006	1.003	1.002	1.000
	$e=E/N^2$	−1.559	−1.552	−1.554	−1.556	−1.558
$1/\ln(1+\sqrt{4})\approx 0.910$						
$q=4$	$1/\beta_c$	0.924	0.916	0.914	0.913	0.913
	$1/\beta_m$	0.934	0.918	0.916	0.915	0.914
	$e=E/N^2$	−1.465	−1.464	−1.466	−1.477	−1.482
$1/\ln(1+\sqrt{6})\approx 0.808$						
$q=6$	$1/\beta_c$	0.817	0.811	0.810	0.809	0.809
	$1/\beta_m$	0.824	0.812	0.810	0.809	0.809
	$e=E/N^2$	−1.344	−1.345	−1.348	−1.349	−1.353
$1/\ln(1+\sqrt{8})\approx 0.745$						
$q=8$	$1/\beta_c$	0.752	0.747	0.746	0.746	0.746
	$1/\beta_m$	0.756	0.746	0.745	0.744	0.744
	$e=E/N^2$	−1.262	−1.255	−1.248	−1.249	−1.250

Table 2. Signal of the order of the transitions.

Categories	Even order transitions	Odd order transitions
Independent	$\frac{\mathrm{d}^{2k}S(E)}{\mathrm{d}E^{2k}}<0$ Negative maximum	$\frac{\mathrm{d}^{2k-1}S(E)}{\mathrm{d}E^{2k-1}}>0$ Positive minimum
Dependent	$\frac{\mathrm{d}^{2k}S(E)}{\mathrm{d}E^{2k}}>0$ Positive minimum	$\frac{d^{2k-1}S(E)}{dE^{2k-1}}<0$ Negative maximum

third-order transitions. Subsequently, the temperature corresponding to this transition can be pinpointed on the curve $\beta(E)$. This method clearly reveals both independent and dependent transitions, with the respective temperatures detailed in table 3. Table 3 presents the locations of third-order transition points obtained by MIPA.

Figures 3(d)–(f) presents the results of the MIPA for the Potts model with $q=6$. Similarly, by employing the previously described method, we have determined the temperatures corresponding to the third-order transitions for the Potts model with $q=3$, 4, 6, and 8 states. These results are presented in table 3.

In table 3, 'NF' denotes that no signal of third-order transitions were detected, but there could be a fourth-order transitions. The numbers in parentheses represent the energy levels at which transition points occur. It is notable that the temperature of

J. Stat. Mech. (2024) 093201

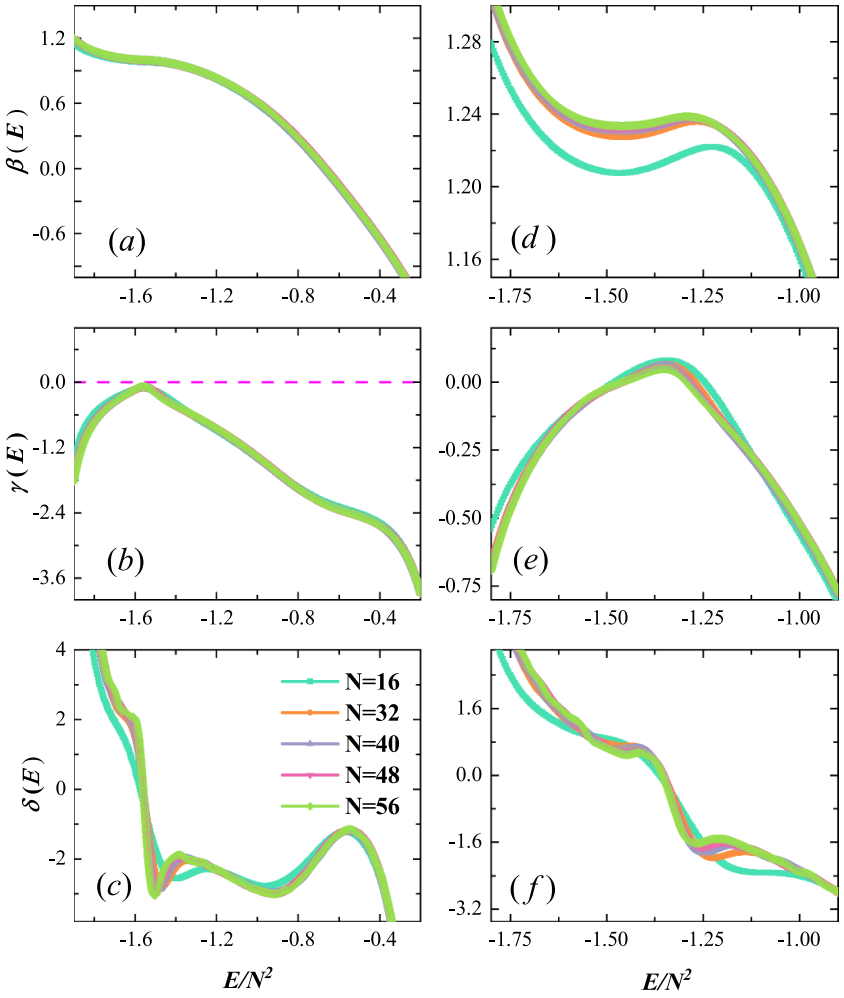

Figure 3. The microcanonical inverse temperature $\beta(E)$, the first and second derivatives of the microcanonical inverse temperature $\gamma(E)$ and $\delta(E)$; $(a)-(c)$ for the $q=4$ state, $(d)-(f)$ for the $q=6$ state in Potts model.

the third-order independent transition for the 6-state Potts model closely approximates that of the dependent transition. This proximity in temperature is attributed to the fact that the 6-state Potts model undergoes a first-order transition at finite size. Furthermore, the non-monotonic backbending of the $\beta(E)$ curve suggests the presence of latent heat and a prolonged temperature-invariant process in the system. However, the closely approximated temperatures correspond to distinctly separate energy levels, indicating that, on a microscopic level, the system occupies two fundamentally different states.

4. Summary

To summarize, we obtained the DOS of the Potts model using the WL and PT methods. The DOS for Potts model with various states was subsequently analyzed using the

J. Stat. Mech. (2024) 093201

Table 3. Locations of the third order transitions for the Potts model.

		$N=16$	$N=32$	$N=40$	$N=48$	$N=56$
$q=3$	$1/\beta_d$	1.164	1.079	1.066	1.049	1.050
	$e=E/N^2$	−1.246	−1.336	−1.354	−1.383	−1.383
	$1/\beta_{\text{in}}$	*NF*	*NF*	*NF*	*NF*	*NF*
$q=4$	$1/\beta_d$	1.005	0.952	0.940	0.938	0.935
	$e=E/N^2$	−1.152	−1.249	−1.283	−1.290	−1.302
	$1/\beta_{\text{in}}$	*NF*	*NF*	*NF*	*NF*	*NF*
$q=6$	$1/\beta_d$	*NF*	0.820	0.814	0.812	0.811
	$e=E/N^2$	*NF*	−1.140	−1.176	−1.201	−1.209
	$1/\beta_{\text{in}}$	*NF*	*NF*	0.813	0.811	0.811
	$e=E/N^2$	*NF*	*NF*	−1.472	−1.457	−1.448
$q=8$	$1/\beta_d$	*NF*	*NF*	*NF*	*NF*	*NF*
	$1/\beta_{\text{in}}$	*NF*	*NF*	0.749	0.749	0.748
	$e=E/N^2$	*NF*	*NF*	−1.378	−1.458	−1.419

MIPA, identifying the positions of transitions of different orders. Comparisons of the micro-positive inflection points with transition positions determined by specific heat under canonical conditions showed good agreement. The results confirm that the DOS obtained from WL is effective for analyzing both first-order and continuous phase transitions and accurately determining the locations of third-order independent and dependent transitions. The presence of higher-order transitions in the Potts model underscores the universality of these transitions to some extent. Notably, the position of higher-order dependent transitions is influenced by the lower-order ones, suggesting that higher-order dependent transitions may act as precursors to critical phase transitions.

MIPA has achieved significant success in addressing third-order transitions in microcanonical systems. Since third-order dependent transition necessitate the existence of lower-order phase transitions, they can be considered precursors to critical phase transitions. In 2022, Sitarachu discovered in a regular system that the third-order dependent transition of the Ising model corresponds to the point where the system size changes most rapidly [40]. This signal persists under the thermodynamic limit and is relatively weak when the system size is small. In recent years, machine learning has proven effective in addressing phase transitions [41, 42], with variational autoregressive networks. showing advantages over traditional methods in small systems. Therefore, our next aim is to use machine learning techniques to identify more precise third-order dependent transition locations and to determine if better probability distributions can be achieved to further investigate the physical implications of these transitions. The universality and physical significance of third-order transitions in various spin systems are crucial for understanding the evolution and prediction of complex systems.

J. Stat. Mech. (2024) 093201

Acknowledgments

We acknowledge the support of NSFC (Nos. 12804257 and 12135003) and 2023–2024 doctoral Interdisciplinary Fund of Beijing Normal University, Zhuhai (No. BNUZHXJC-31). The computing resource is supported by Interdisciplinary Intelligence Super-Computer Center of Beijing Normal University, Zhuhai.

References

[1] Pathria R K 2001 *Statistical Mechanics* (Elsevier)
[2] Onsager L 1944 *Phys. Rev.* **65** 117–49
[3] Toledano P and Toledano J 1987 *Landau Theory of Phase Transitions, the: Application to Structural, Incommensurate, Magnetic and Liquid Crystal Systems* (*Lecture Notes in Physics*) (World Scientific)
[4] Wilson K G 1983 *Rev. Mod. Phys.* **55** 583–600
[5] Giansanti A 2008 *AIP Conf. Proc.* **36** 155–64
[6] Bachmann M 2014 *Thermodynamics and Statistical Mechanics of Macromolecular Systems* (Cambridge University Press)
[7] Dorogovtsev S N, Goltsev A V and Mendes J F F 2008 *Rev. Mod. Phys.* **80** 1275–335
[8] Chamberlin R V 2014 *Entropy* **17** 52–73
[9] Bedeaux D, Kjelstrup S and Schnell S K 2020 *Nanothermodynamics–General Theory* (PoreLab)
[10] Gross D H E 2001 *Microcanonical Thermodynamics* (World Scientific)
[11] Junghans C, Bachmann M and Janke W 2006 *Phys. Rev. Lett.* **97** 218103
[12] Qi K and Bachmann M 2018 *Phys. Rev. Lett.* **120** 180601
[13] Beale P D 1996 *Phys. Rev. Lett.* **76** 78
[14] Sitarachu K, Zia R and Bachmann M 2020 *J. Stat. Mech.* 073204
[15] Qi K, Liewehr B, Koci T, Pattanasiri B, Williams M J and Bachmann M 2019 *J. Chem. Phys.* **150** 054904
[16] Liu W, Wang F, Sun P and Wang J 2022 *J. Stat. Mech.* 093206
[17] Aierken D and Bachmann M 2023 *Phys. Rev.* E **107** L032501
[18] Williams M J 2023 *Polymers* **15** 3870
[19] Bel-Hadj-Aissa G 2020 *Phys. Lett.* A **22** 126449
[20] Bel-Hadj-Aissa G, Gori M, Penna V, Pettini G and Franzosi R 2020 *Entropy* **22** 380
[21] Potts R 1952 *Math. Proc. Camb. Phil. Soc.* **48** 106–9
[22] Ising E 1925 *Z. Phys.* **1925** 253–8
[23] Wu F Y 1982 *Rev. Mod. Phys.* **54** 235–68
[24] Baxter R J 2007 *Exactly Solved Models in Statistical Mechanics* (Courier)
[25] Reichardt J and Bornholdt S 2004 *Phys. Rev. Lett.* **93** 218701
[26] Guimera R, Sales-Pardo M and Amaral L A N 2004 *Phys. Rev.* E **70** 025101
[27] Lambiotte R A M and Ausloos M 2005 *Phys. Rev.* E **72** 066107
[28] Stauffer D and Solomon S 2007 *Eur. Phys. J.* B **57** 473–9
[29] Belousov R, Savino S, Moghe P, Hiiragi T, Rondoni L and Erzberger A 2024 *Phys. Rev. Lett.* **132** 248401
[30] Zhu X, Gerstein M and Snyder M 2007 *Genes Dev.* **21** 1010–24
[31] Besag J 1986 *J. R. Stat. Soc.* B **48** 259–79
[32] Wang F and Landau D P 2001 *Phys. Rev. Lett.* **86** 2050–3
[33] Marinari E and Parisi G 1992 *Europhys. Lett.* **19** 451–8
[34] Hukushima K and Nemoto K 1996 *J. Phys. Soc. Japan* **65** 1604–8
[35] Cunha-Netto A G, Caparica A A, Tsai S H, Dickman R and Landau D P 2008 *Phys. Rev.* E **78** 055701
[36] Vogel T, Li Y W, Wüst T and Landau D P 2013 *Phys. Rev. Lett.* **110** 210603
[37] Vogel T, Li Y W, Wüst T and Landau D P 2014 *Phys. Rev.* E **90** 023302
[38] Newman M E J and Barkema G T 2001 *Monte Carlo Methods in Statistical Physics* (Journal of the American Statistical Association)
[39] Grotendorst J, Marx D and Muramatsu A 2002 *Quantum Simulations of Complex Many-Body Systems: From Theory to Algorithms* (ReaearchGate)
[40] Sitarachu K and Bachmann M 2022 *Phys. Rev.* E **106** 014134
[41] Tang Y, Liu J, Zhang J and Zhang P 2024 *Nat. Commun.* **15** 1117
[42] Wu D, Wang L and Zhang P 2019 *Phys. Rev. Lett.* **122** 080602

J. Stat. Mech. (2024) 093201